

Estimating a Volumetric Backscatter Coefficient from In-Situ Measurements on the Greenland Ice Sheet

J. Munk¹, K. Jezek², F. Baumgartner³, S. P. Gogineni⁴, R. R. Forster⁵ and I. H. H. Zabel⁶

^{1,2,3,5,6}Byrd Polar Research Center, The Ohio State University, 1090 Carmack Rd., Columbus, Ohio 43210. Tel: (614) 292-1063, Fax: (614) 292-4697.

³Currently at the Department of Geology and Geotechnical Engineering, Denmark's Technical University, DK-2800 Lyngby, Denmark.

⁴Radar Systems and Remote Sensing Laboratory, University of Kansas, 2291 Irving Hill Rd., Lawrence, Kansas 66045. Tel: (785) 864-7734, Fax: (785) 864-7789

⁵Currently at the Department of Geography, University of Utah, 260 South Central Campus Dr., Salt Lake City, UT 84112-92115. Tel: (810) 581-3661, Fax: (810) 581-8219.

⁶Currently at M.I.T. Lincoln Laboratory, 244 Wood Street, Lexington, MA 02420. Tel: (781) 981-2732, Fax: (781) 981-2780.

Email: ¹munk@frostdy.mps.ohio-state.edu, ²jezek@iceberg.mps.ohio-state.edu, ³iggfb@pop.dtu.dk, ⁴gogineni@rsl.ukans.edu, ⁵forster@geog.utah.edu and ⁶zabel@ll.mit.edu.

Abstract— We obtained in-situ radar backscatter data at several sites on the Greenland Ice Sheet to better relate scattering signatures to firn physical properties. Backscatter measurements were made using an ultra-wide band radar system (.5-18 GHz) for incidence angles between 0 and 50 degrees, with respect to the snow surface. For large angles of incidence ($> 25^\circ$) the measured backscatter is dominated by volumetric scattering, as opposed to surface and specular backscatter occurring at near normal incidence. Using the data we present a method for estimating the volumetric backscatter coefficient as a function of depth in firn. Results show trends consistent with both seasonal variations and long-term grain growth, which is primarily influenced by the accumulation rate

I. INTRODUCTION

IN arctic regions, space-borne radar has been successfully used to map the extent of polar ice sheets, define margins between various snow zones and, in dry snow zones, determining accumulation rates. Algorithms to extract these geophysical variables are largely based on empirical models. To better understand firn backscatter and to develop more rigorous algorithms, *in-situ* radar measurements were made at several sites on the Greenland ice sheet. An ultra-wide band radar system was used to collect backscatter data in the frequency domain which were subsequently transformed into time/depth domain. Unlike space-borne radar, which only measures a single average scattering cross section, we use our *in-situ* data to determine the backscatter with depth. This can then be related to physical properties of the firn.

II. FORMULATION

The power return resulting from an incremental volume is given by,

$$d^3P_r = \frac{P_t \lambda^2}{(4\pi)^3} G_0^2 g^2(\theta, \phi) \sigma_v \frac{e^{-2\tau}}{R^4} dV, \quad (1)$$

where P_t is the transmitted power, G_0 is the maximum antenna gain, $g(\theta, \phi)$ is the normalized antenna gain function, λ is the wavelength, σ_v is the volumetric backscatter and R is the range from the antenna to the volume $dV = R^2 dR d\Omega$, with $d\Omega \equiv \sin\theta d\theta d\phi$. The angles θ and ϕ are referenced to

This work is supported by NASA's Polar Program.

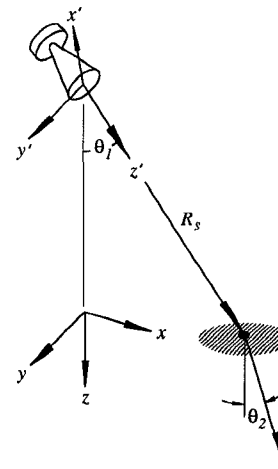


Fig. 1. Antenna illuminating snow surface at $z = 0$, with the shaded region, A_{ill} , corresponding to the main antenna beam.

the primed coordinates, which are centered at the antenna feed, as shown in figure 1. The attenuation factor

$$\tau \equiv \int_{R_s}^R \kappa_e dR, \quad (2)$$

where κ_e is the extinction coefficient and R_s is the range from the antenna to the snow surface. The extinction coefficient describes attenuation due to propagation within the firn and is comprised of a scattering and absorption term such that $\kappa_e \equiv \kappa_s + \kappa_a$. For spherical scatterers the absorption and scattering terms are given by Mie [2], [3].

In terms of the solid angle $d\Omega$, equation (1) is given by

$$d^2P_r = \frac{P_t \lambda^2}{(4\pi)^3} G_0^2 g^2(\theta, \phi) \gamma d\Omega, \quad (3)$$

where

$$\gamma \equiv \int_{R_s}^{\infty} \sigma_v \frac{e^{-2\tau}}{R^2} dR. \quad (4)$$

Assuming σ_v varies only with depth, and substituting,

$$\Delta R \equiv R - R_s = z \sec \theta_2,$$

yields the more general expression

$$\gamma = \int_0^\infty \sigma_v(z) \frac{e^{-2\tau(z)}}{(R_s + z \sec \theta_2)^2} \sec \theta_2 dz, \quad (5)$$

where

$$\tau(z) = \int_0^z \kappa_e(z' \sec \theta_2) \sec \theta_2 dz', \quad (6)$$

with θ_1 and θ_2 related through Snell's law (see fig. 1). In equation (5), the volumetric backscatter coefficient is modulated by a spherical spreading term, and by the exponential term related to the extinction coefficient. Scattering from individual snow grains results in attenuation in the direction of wave propagation, and contributes to the measured backscatter.

Within a narrow frequency range, the antenna gain function can be assumed approximately constant. Letting the wavelength, λ , equal that of the center frequency, equation (3) can be expressed as $d^2 P_r \propto \gamma$ or, under a pencil beam approximation simply $P_r \propto \gamma$. Thus,

$$P_r = K_f \gamma, \quad (7)$$

with K_f a constant, valid for a given frequency range. Performing a calibration using a Luneberg lens yields [4],

$$K_f = \frac{P_l R_l^4}{\sigma_l} \frac{A_{ill}}{R_s^2} \cos \theta_1, \quad (8)$$

where P_l , R_l and σ_l are the return power, range and RCS of the lens, with A_{ill} , θ_1 and R_s as shown in figure 1.

In terms of firn depth, the power can be expressed as,

$$P_r \equiv \int_0^\infty P_r(z) dz = K_f \gamma, \quad (9)$$

where

$$z = \frac{vt}{2} \cos \theta_2 \quad (10)$$

with the velocity $v = c/\sqrt{\epsilon}$. For snow densities typical of the upper firn, the relative permittivity $\epsilon \approx 1.7$ [5], where $\epsilon \equiv \epsilon' + j\epsilon''$ with $\epsilon'' \ll \epsilon'$, so that it can be neglected in determining v . Equating integrands in equation (9) yields,

$$P_r(z) = K_f \sigma_v(z) \frac{e^{-2\tau(z)} \sec \theta_2}{(R_s + z \sec \theta_2)^2}, \quad (11)$$

or, in terms of σ_v ,

$$s(z) \equiv K_f \sigma_v(z) e^{-2\tau(z)} = \frac{P_r(z)}{\sec \theta_2} (R_s + z \sec \theta_2)^2, \quad (12)$$

where all components on the right-hand side are known. In equation (12), the effects of spherical spreading are effectively removed by gaining the power as a function of depth/time.

Refraction at the air-snow interface modifies the spherical spreading, which can be accounted for by replacing R_s in equation (12) with \tilde{R}_s , as illustrated in figure 2. For small $\delta\theta_1$,

$$\tilde{R}_s = R_s \sqrt{\epsilon} \left(\frac{\cos \theta_2}{\cos \theta_1} \right)^2. \quad (13)$$

The range modification introduced by the snow can be significant. For example, with $\theta_1 = 50^\circ$ and $\epsilon = 1.7$, we obtain $\tilde{R}_s \approx 2.1R_s$, (see fig. 2).

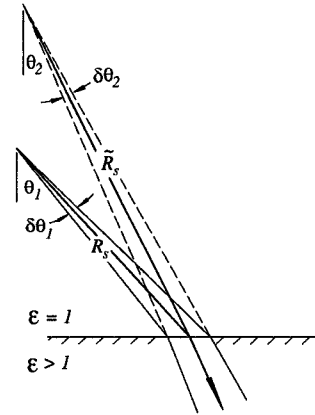


Fig. 2. Effects of a half-space on geometrical spreading.

III. RESULTS

An ultra-wide band radar system (0.5-18 GHz), was used to collect backscatter data at several sites on the Greenland Ice Sheet. Data were obtained in the frequency domain in $N = 1601$ evenly spaced increments of $\Delta f = 12.1$ MHz, beginning at 570 MHz. The frequency increment Δf , limits the maximum range into the snow such that

$$z_{max} = \frac{1}{\Delta f} \frac{v}{2} \cos \theta_2, \quad (14)$$

where $1/\Delta f = t_{max}$.

The return power as given in equation (1), is expressed in terms of volumetric scattering, which is known to be incoherent. For angles $\theta_1 > 30^\circ$ the return power generally results from volumetric scattering [6]. To determine P_r , a coherent signal component, primarily comprised of a system response, was calculated and subsequently removed from the measured data. The coherent signal is obtained by averaging the data from the different locations within each site. The data were then demodulated and windowed using a bandwidth of $f_{bw} = 1.0$ GHz. In the time-domain the power return was obtained using the Fourier transform, and then averaging the resulting incoherent power returns from the three locations. Plots of $s(z)$ obtained from the NASA-U site are shown in figure 3, for center frequencies of 5.3 and 17.0 GHz, and with $\theta_1 = 50^\circ$. The data have been shifted in time/depth such that $t = 0$ corresponds to $z = 0$.

Limitations imposed by the frequency step, Δf , can result in spatial aliasing, so that events occurring before $t = 0$ or after t_{max} , simply wrap within this range. As a result, system artifacts not removed from the data are shifted and inadvertently gained with depth. This is shown in figure 3(a), where the sharp increase beyond 6.8 meters is likely due to antenna coupling. At higher frequencies the narrower antenna beam-width makes this component less significant, as illustrated in figure 3(b). The strong signal returns at depth (figures 3(a) and 3(b)) indicate that a smaller frequency step could have been used to resolve deeper layers.

The data shown in figure 3 exhibits significant variability which, is likely due to the number of frequencies ($f_{bw}/\Delta f \approx$

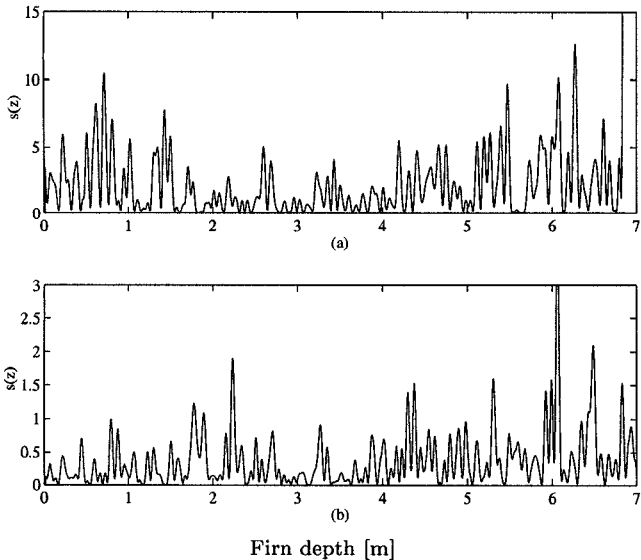


Fig. 3. Plots of $s(z)$ from NASA-U site with $\theta_1 = 50^\circ$, for (a) 5.3 GHz, and (b) 17 GHz (bandwidth=1.0 GHz).

82) used in generating $s(z)$, and the random nature of the scatterers comprising the firn. A smoothed version of the data are obtained by convolving $s(z)$ with the filter $h(z)$ such that,

$$s_h(z) = s(z) * h(z) \equiv \int s(z')h(z-z')dz', \quad (15)$$

where $s_h(z)$ are the smoothed data, and

$$h(z-z') \equiv \frac{1}{A_f} \exp\left(-2\left[\frac{z-z'}{z_{bw}}\right]^2\right). \quad (16)$$

The filter bandwidth is given by z_{bw} , with the additional term

$$A_f \equiv \int_{-\infty}^{+\infty} \exp\left(-2\left[\frac{z-z'}{z_{bw}}\right]^2\right) dz, \quad (17)$$

included as a normalization factor.

A smoothed version of $s(z)$ (fig. 3) is shown in figure 4, where $s_h(z)$ was obtained using $z_{bw} = 0.5$ m. With spherical spreading effects removed, attenuation of $s_h(z)$ results entirely from the term $e^{-2\tau}$. Figures 4(a) and 4(b), suggest that the trend for $s_h(z)$ is approximately constant or slightly increasing with depth. With the loss factor $e^{-2\tau}$ removed, the remaining signal should show an increasing trend, indicating an increase in snow grain size and/or density with depth.

Based on $\delta^{18}O$ analyses of 3 cores from the NASA-U sites, the upper 6.5 meters of firn represent approximately 9 years of accumulation. Figure 4(c) shows the $\delta^{18}O$ measurements from one of the NASA-U cores, where the peaks correspond to late summer seasons. At 17 GHz, where the beam-width is relatively narrow, comparisons between figures 4(b) and 4(c) reveal similarities in shape. Spatial variations in firn stratigraphy between the 3 NASA-U sites and the location where radar data were collected may result in some of the non-similarities. We suggest a correlation between grain size and $\delta^{18}O$, where larger snow grains, typically associated with summer warming, result in increased

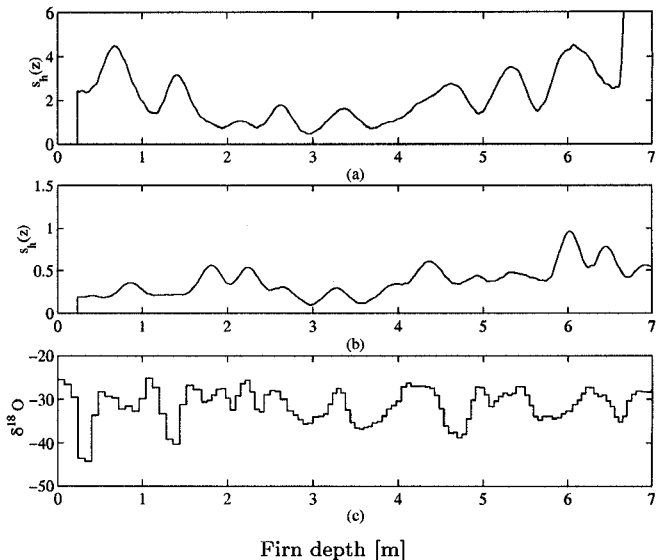


Fig. 4. Plots from NASA-U site for, (a) $s_h(z)$ at 5.3 GHz ($\theta_1 = 50^\circ$) (b) $s_h(z)$ at 17 GHz ($\theta_1 = 50^\circ$) and (c) $\delta^{18}O(z)$.

backscatter, as predicted by radiative transfer theory. At lower frequencies the return signal is complicated by the beam-width ($\approx 25^\circ$ at 5.3 GHz for our antenna), where the backscatter can result simultaneously from various depths.

IV. CONCLUSIONS

In-situ radar measurements reveal both seasonal and long-term trends in the data. For large angles of incidence, where volume scattering dominates, an increase in backscatter with depth indicates an increase in grain size and/or density with depth. Annual variations in firn may also be evident in the data as comparisons between $s_h(z)$ and $\delta^{18}O(z)$ suggest, provided the antenna beam-width is sufficiently narrow. The results further suggest that, at large incidence angles, radiative transfer algorithms based on volume scattering, such as that used by Forster [1], provide a reasonable model for firn scattering.

ACKNOWLEDGEMENT

The authors thank Dr. Ellen Mosley-Thompson of the Byrd Polar Research Center for providing the ice core data.

REFERENCES

- [1] R. R. Forster, K. C. Jezek, J. F. Bolzan, F. Baumgartner and S. P. Gogineni, 1999, "Relationships between radar backscatter and accumulation rates on the Greenland ice sheet", *International Journal of Remote Sensing*, **20** (15), 3131-3147.
- [2] F. T. Ulaby, R. K. Moore and A. K. Fung, *Microwave Remote Sensing*, vol. I. Artech House, Inc., 1981.
- [3] H. C. van de Hulst, *Light Scattering by Small Particles*. New York: John Wiley and Sons, Inc., 1957.
- [4] F. Baumgartner, K. Jezek, R. R. Forster, S. P. Gogineni and I. H. H. Zabel, "Spectral and angular ground-based backscatter measurements of Greenland snow facies", *IGARSS 99 Proceedings*, pp 1053-1055, June 1999.
- [5] M. E. Tiuri, A. H. Sihvola, E. G. Nyfors and M. T. Hallikainen, "The complex dielectric constant of snow at microwave frequencies", *IEEE Journal of Oceanic Engineering*, vol. OE-9 no. 5, pp 377-382, 1984.
- [6] F. T. Ulaby, R. K. Moore and A. K. Fung, *Microwave Remote Sensing*, vol. III. Artech House, Inc., 1986.